Magnetic and Electrocatalytic Properties of Nanoscale Cobalt Boride, Co₃B

Anne-Marie Zieschang, ¹ Joshua D. Bocarsly, ² Jona Schuch, ³ Christina V. Reichel, ¹ Bernhard Kaiser, ³ Wolfram Jaegermann, ³ Ram Seshadri, *, ² Barbara Albert*, ¹

ABSTRACT: The use of low-temperature solution synthesis followed by a brief annealing step allows metastable single-phase Co_3B nanoparticles to be obtained, with sizes ranging from 11 nm to 22 nm. The particles are ferromagnetic with a saturation magnetization of 91 A m² kg⁻¹ (corresponding to 1.02 μ_B/Co) and a coercive field of 0.14 T at 5 K, retaining the semi-hard magnetic properties of bulk Co_3B . They display a magnetic blocking temperature of 695 K and a Curie temperature near 710 K, but the measurement of these high-temperature properties was complicated by decomposition of the particles at these high temperatures. Additionally, the nanoparticles of Co_3B were investigated as an electrocatalyst in the oxygen evolution reaction and showed a low onset potential of 1.55 V vs. RHE. XPS measurements were performed before and after the electrocatalytic measurements to study the surface of the catalyst, to pinpoint what appear to be the active surface species.

Introduction

With growing interest in transition metal borides, ¹⁻¹⁶ especially cobalt borides, ^{2,17-22} as catalyst and electrocatalyst materials, the importance of the synthesis of phase-pure nanoscale transition metal borides increases. These materials provide high surface areas compared to bulk metal borides and show excellent catalytic activity. However, to date, many transition metal borides can only be obtained as bulk materials or amorphous powders. To produce catalytic materials, the so-called top-down approach is usually carried out using ball-milling to grind bulk materials into smaller particles. Especially for hard materials such as borides, this can introduce impurities into the material and often leads to broad particle size distributions which can be detrimental to the catalytic activity. A more sophisticated approach are bottom-up methods, to build the nanoparticles from an atomic level. For transition metal boride nanoparticles, they often include a reaction of alkali metal tetrahydridoborates and transition metal salts either in water, ^{7,23-29} organic solvents, ^{27,30,31} or salt-melts. ^{32,33} Another reaction of transition metal salts with elemental boron in tin melts was described recently. ³⁴ A review of synthesis methods for nanoscale metal borides can be found in literature. ¹

¹ Eduard-Zintl-Institute of Inorganic and Physical Chemistry, Technische Universität Darmstadt, Alarich-Weiss-Str. 12, 64287 Darmstadt, Germany

² Department of Chemistry & Biochemistry, Materials Department, and Materials Research Laboratory, University of California, Santa Barbara, Santa Barbara California 93106, United States

³ Institute of Materials Science (Surface Science Division), Technische Universität Darmstadt, Jovanka-Bontschits-Str. 2, 64287 Darmstadt, Germany

Previously, we reported the formation of metastable nanoparticles of Ni₇B₃ at room temperature by using a solution synthesis route.²³ Here, we report on the preparation of metastable single-phase nanoparticles of Co₃B for the first time, applying a similar approach. Co₃B is often found as a side-product in precipitation syntheses^{26,31,35,36} or can be prepared as bulk material by induction melting of the elements and subsequent heat treatment or reaction of the elements in silica ampules.³⁷⁻³⁹ It crystallizes in the orthorhombic Fe₃C structure type (space group *Pnma*). The unit cell consists of isolated boron atoms, which are enclosed by tricapped trigonal prisms consisting of nine cobalt atoms as shown in Figure 1 (a).

Another cobalt boride, Co₂B, has already shown high efficiency as an electrocatalyst material for the oxygen evolution reaction^{2,7,40} and high selectivity as a catalyst in reactions such as the liquid-phase hydrogenation of citral.^{19,41} Amorphous Co-B powders are possible high capacity anode materials for battery applications.⁴² Mixtures of Co₂B and Co₃B were tested for the oxidative dehydrogenation of propane recently and showed high olefin selectivity.⁴³ For catalysis, amorphous products, mixtures of Co-B compounds or poorly-crystalline materials were often used.^{2,6,17,21,22,40} However, the use of well-defined binary compounds is essential to improve the understanding of the influence of structure and catalyst composition on the catalytic properties. Because phase-pure Co₃B nanoparticles were so far inaccessible, there are no reports on their catalytic properties.

Furthermore, transition metal-based compounds other than oxides, especially borides, have attracted attention because of their magnetic properties. ^{30,39,44-51} Due to its ferromagnetic properties, which are intermediate between those of a hard magnet and a soft magnet, ³⁹ nanoscale Co₃B may also be used in magnetic switches, data storage and biomedical applications. Nanocompositing magnetically semi-hard magnetic materials such as Co₃B or (Fe_xCo_{1-x})₃B with magnetically hard (but lower moment) magnetic materials such as Mn-Ga or Mn-Bi has been proposed as a route to transition metal-based permanent magnets that combine high saturation magnetization and high coercivity. ³⁹ The development of high-quality magnetic nanoparticles will enable the preparation of these types of nanocomposites through spark plasma sintering or hot-pressing.

In this work, nanoscale and pure Co₃B was prepared through the reaction of lithium tetrahydridoborate and cobalt(II)-bromide in tetrahydrofuran with subsequent washing and annealing. Transmission electron microscopy (TEM) was used to analyze the nanostructure of the samples. High-resolution synchrotron powder diffraction and magnetic studies confirmed that they were single-phase. Furthermore, the particles were analyzed as a catalyst material for electrochemical water splitting. The surface was studied using XPS before and after electrochemical measurements.

Experimental Section

Synthesis. The glassware was heated *in vacuo* and then flushed with argon three times to remove all traces of water and oxygen. All synthesis and characterization steps were performed without exposure of the samples to air unless otherwise stated. Tetrahydrofuran was degassed using the freeze-pump-thaw

method prior to the synthesis. 20 mmol (1 eq.) of cobalt(II)-bromide (Sigma Aldrich, 99 %) were dissolved in 50 ml of tetrahydrofuran and 46 mmol (2.3 eq.) of lithium tetrahydridoborate (Sigma Aldrich, \geq 95 %) were dissolved in 20 ml of tetrahydrofuran. The solution of lithium tetrahydridoborate was added to the solution of cobalt(II)-bromide quickly. The solution changed color from blue to black immediately and was stirred for two hours at room temperature. The black precipitate was filtered and washed five times with 20 ml of tetrahydrofuran. The sample was rinsed with 20 ml of ethanol, added quickly to the precipitate on the frit, which caused it to heat up. The precipitate was again filtrated and dried *in vacuo* for eight hours. It is pyrophoric and exhibits ferromagnetic behavior. Filtration and washing steps were also carried out under an argon atmosphere using Schlenk techniques. The black powder was heated to 773 K within an hour and then treated at 773 K for two hours *in vacuo*, yielding Co₃B nanoparticles.

Structural characterization. X-ray powder diffraction data were collected at room temperature by a Stoe STADI P powder diffractometer with MoK $_{\alpha 1}$ radiation (Ge(111) monochromator, $\lambda = 0.7093$ Å, Debye-Scherrer geometry). Samples were sealed in glass capillaries to avoid exposure to air.

High-resolution synchrotron powder diffraction data were collected at 295 K using beamline 11-BM at the Advanced Photon Source (APS), Argonne National Laboratory, using an average wavelength of 0.412802 Å. To avoid exposure to air, samples were loaded in a glovebox into 0.8 mm diameter Kapton capillaries, which were sealed on each end using epoxy.

Rietveld refinement was performed using the program TOPAS Academic. The data was fit using a purely Lorentzian Stephens peak profile for the microstrain,⁵² and a standard Lorentzian size broadening term. The refinement of the size broadening term was used to determine the size of the coherent scattering regions (volume-weighted column height).

Magnetic measurements. Magnetization measurements were performed using a SQUID magnetometer (Quantum Design MPMS-3) equipped with a high-temperature oven option, which allows for Vibrating Sample Magnetometer (VSM) measurements between 2 K and 1000 K. In order to avoid exposing the nanoparticles to air or water while performing the high-temperature measurements (300 K and above), a few milligrams of nanoparticles were loaded into a small section of silver tube (2.8 mm OD) in an argon glovebox. The ends of tubes were crimped and the tube was flattened into an air-tight packet. The packet was removed from the glovebox and cemented to the oven sample heater of the magnetometer, which was then wrapped in copper foil and placed in the sample chamber (He/vacuum environment). We have previously employed this technique successfully to measure the high-temperature magnetic properties of air sensitive nanoparticles.⁴⁷ For the low-temperature measurements (300 K and below), nanoparticles were loaded into a closed polypropylene capsule in the glovebox, which was then removed from the glovebox, carefully weighed, and quickly placed in the MPMS sample chamber. The mass and 300 K moment of the low-temperature sample was used to calibrate the moment of the high-temperature sample.

Transmission electron microscopy. A (scanning) transmission electron microscope (STEM, JEOL JEM 2100F, 200 kV) was used to determine the microstructure and chemistry on the nanometer scale. A transfer specimen holder model (Gatan 648) was used to avoid exposure to air. The TEM grids were prepared in a glove box by placing the sample in a mortar and carefully pulling the TEM grid through the powder.

Energy-dispersive X-ray spectroscopy. A scanning electron microscope (JEOL JSM 6400) was used at 20 kV with a detector (EDAX Apollo X) for the energy-dispersive X-ray spectroscopy (EDS). Samples were prepared in air on adhesive carbon pads.

X-ray photoelectron spectroscopy. XPS measurements were performed using monochromatic $Al_{K\alpha}$ radiation (XR 50, SPECS Surface Nano Analysis GmbH). A hemispherical electron analyzer (PHOIBOS 150, SPECS Surface Nano Analysis GmbH) was used, calibrated with the core lines of copper, silver, and gold. Prior to the electrochemical measurements, samples of Co_3B were embedded into indium foil. Only moderate pressure was applied to embed the powder into the indium foil in order to keep the crystallites intact.

Electrode assembly. The powder of Co₃B (5 mg mL⁻¹) was added to a mixture of 45 % ethanol, 45 % ultra-pure distilled water, and 10 % Nafion (Aldrich Chemistry). The ink was blended using an ultrasonic bath for at least 30 min. Glassy carbon (HTW GmbH) was used as a substrate material, sanded with abrasive silicon carbide paper (P400, P1000, P1500, P2000, P2500 grit size, Starcke) and polished with Al₂O₃ paste (1 μm, 0.05 μm grit size, Buehler). The substrate was cleaned with ethanol and ultrapure distilled water for 10 min each in an ultrasonic bath. 15 μL of the resulting ink were loaded onto the glassy carbon substrate with an Eppendorf pipette and dried for at least one hour under ambient conditions.

Electrochemical measurements. The catalytic performance tests with respect to the oxygen (OER) and hydrogen evolution reaction (HER) were conducted using a potentiostat (GAMRY Interface 1000E) in a three-electrode setup with a Hg/HgO (1 M NaOH) reference electrode in 1 M KOH (Carl Roth) solution. The catalyst was first activated using cyclic voltammetry (CV) between 1 and 1.5 V with a scan rate of 100 mV s⁻¹ until no further shifts were observed in the voltammograms. The activity was then obtained by a further CV measurement between 1 and 1.8 V with a scan rate of 10 mV s⁻¹ for the OER. The HER activity was determined by a full range CV curve between -0.5 V and 1.8 V with a scan rate of 50 mV s⁻¹. Electrochemical impedance spectroscopy (EIS; 100 kHz–1 Hz) was used to obtain the setup resistance for iR compensation. In this work all electrochemical plots are calibrated to the reversible hydrogen electrode (RHE).

Results and discussion

The reaction of cobalt(II)-bromide with lithium tetrahydridoborate in degassed tetrahydrofuran resulted in single-phase, crystalline Co₃B according to X-ray diffraction after annealing at 773 K (Figure 1 (b), Table 1). Synchrotron data suggests an average coherent scattering region between 12 and 22 nm, which varies slightly based on how the refinement is carried out. There is no evidence of any side-phases. The

crystallographic data of the refined structure can be found in the Supporting Information. The refined lattice parameters are comparable to values described in literature.⁵³

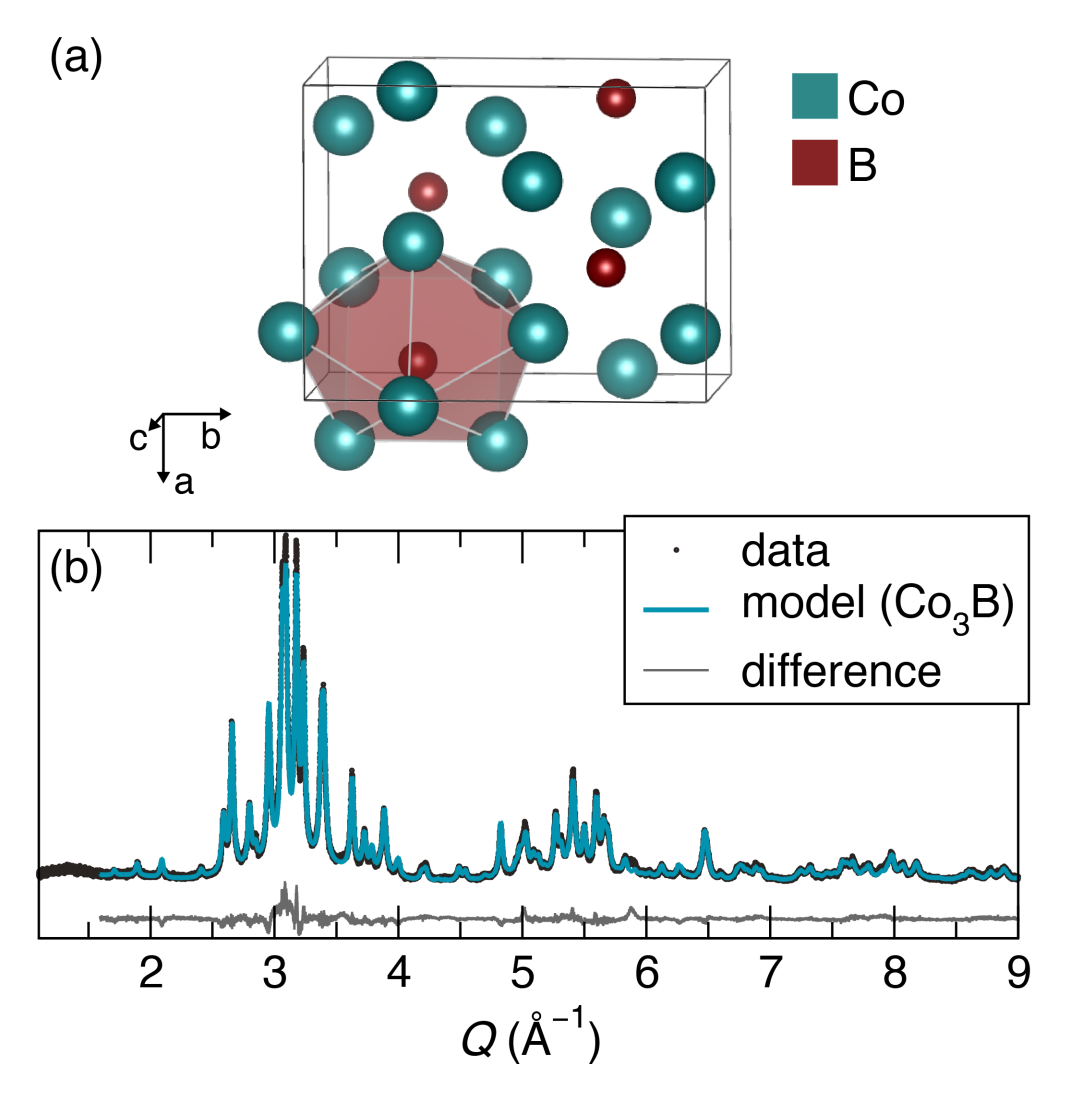


Figure 1: (a) Structure of Co₃B with teal cobalt and red boron atoms. Isolated boron atoms are enclosed by tricapped trigonal prisms. (b) High-resolution synchrotron powder diffraction data of Co₃B.

Table 1: Rietveld refinement data of high-resolution synchrotron powder diffraction data of Co₃B.

Temperature / K	295
Space group	Pnma
a / Å	5.2132(2)
b / Å	6.6375(2)
c / Å	4.4113(1)
$V/$ $\mathring{\mathbf{A}}^3$	152.640(5)
$\mathbf{R}_{\mathbf{exp}}$	5.195
$\mathbf{R}_{\mathbf{wp}}$	7.439
GOF	1.432

The TEM investigation demonstrated that the nanoparticles were highly agglomerated due to their ferromagnetic properties and small particle size. Figure 2 shows bright-field images of three Co₃B

agglomerates after annealing at 773 K. The average particle diameter as determined from TEM bright-field images was 11 (\pm 5) nm (see Supporting Information, Figure S1) and was slightly smaller than the crystallite size determined by X-ray diffraction. However, this may be misleading as only thin parts of the agglomerates could be analyzed using TEM, but thicker parts may contain larger particles. Prolonged exposure of the particles to the electron beam resulted in the decomposition of the metastable compound.

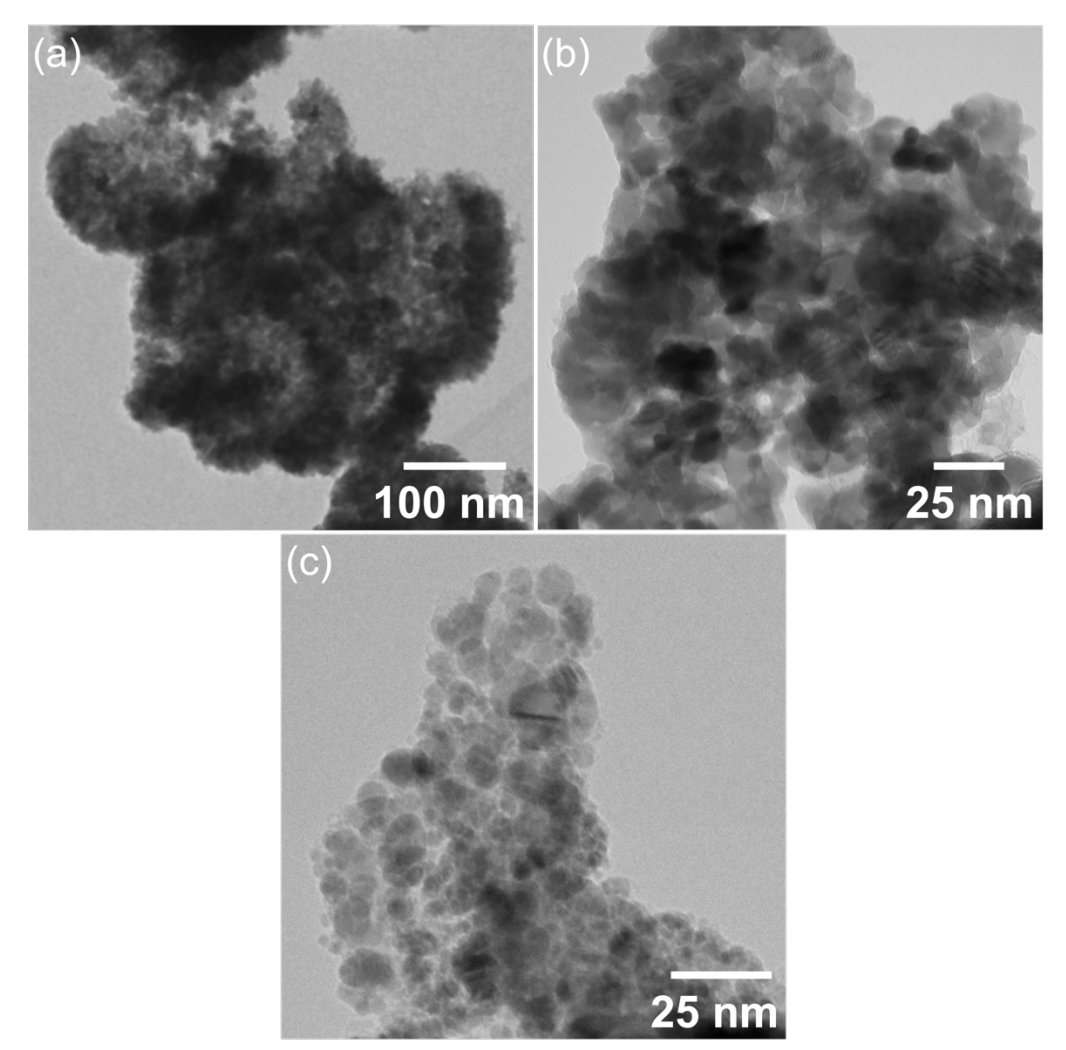


Figure 2: (a), (b) and (c) Bright-field images of agglomerates of nanoparticles of Co₃B.

EDS analysis of the samples in a scanning electron microscope revealed no impurities of other metals. Due to the low atomic number of boron, the boron content of the sample was not analyzed. Apart from cobalt and boron, only small amounts of carbon and oxygen were detected, most likely caused by the adhesive carbon pads on which the sample is prepared and the preparation of the sample in air for SEM analysis.

Interestingly, the washing procedure had a significant impact on the composition of the product. To obtain phase-pure Co₃B, it was essential that the sample was only washed once with ethanol and that the solvent was added quickly to the precipitate. Any deviation from the washing procedure resulted in mixtures of the cobalt borides CoB, Co₂B and Co₃B as well as elemental cobalt. Glavee et al.²⁶ describe that partial conversion of Co₂B to Co is crucial to obtaining Co₃B through thermal processing by reaction of Co₂B and Co nanoparticles. In the present work, this may have been achieved by addition of ethanol

to the precipitated amorphous product. Furthermore, Glavee et al.²⁶ assume that the main product of precipitation synthesis in non-aqueous media is metallic cobalt. However, before washing with ethanol the samples described in this work did not react to an external magnet, which excludes cobalt as the main product. After the washing, the precipitate exhibited ferromagnetic behavior. If the sample was washed with tetrahydrofuran instead of ethanol and then heat-treated at 873 K for two hours, the main product was CoB and the product was much less crystalline. A variation of the ratio of LiBH₄ to Co²⁺ led to mixtures of different cobalt borides and elemental cobalt.

Heat treatment of the Co₃B nanoparticles at 873 K instead of 773 K synthesis led to the formation of cobalt as a side-phase ($Fm\overline{3}m$, see Supporting Information, Figure S2). Corrias et al.³⁵ also described the decomposition of Co₃B into the more stable Co₂B and segregation of metallic cobalt above 873 K. The phase-diagram by Omori et al.³⁸ suggests that Co₃B is only stable between 1118 K and 1383 K. Therefore, we tried to obtain more crystalline samples by heating the sample to 1223 K for six hours in a silica ampule and quenching after the heat treatment. Although the XRD reflections of Co₃B seemed sharper, and the sample therefore more crystalline, the procedure also resulted in a partial decomposition of Co₃B into Co ($Fm\overline{3}m$ and $P6_3/mmc$) and Co₂B (I4/mcm). Therefore, we used the samples as obtained from the initial 773 K heat treatment for all further characterization.

The nanoparticles of Co₃B showed ferromagnetic behavior, with magnetic hysteresis observed (Figure 3) with a coercive field $\mu_0 H_C = 0.13$ T at 300 K and 0.14 T at 5 K. The magnetic saturation at 5 K and 5 T was 1.02 μ_B /Co (91.0 A m² kg⁻¹), which is slightly lower than in the bulk material (1.1 μ_B /Co), ^{53,54} as is often observed in magnetic nanoparticles. ^{47,55} This measured magnetic moment is consistent with the lack of metallic cobalt in the samples, which shows a moment of 1.7 μ_B /Co. ⁵⁶

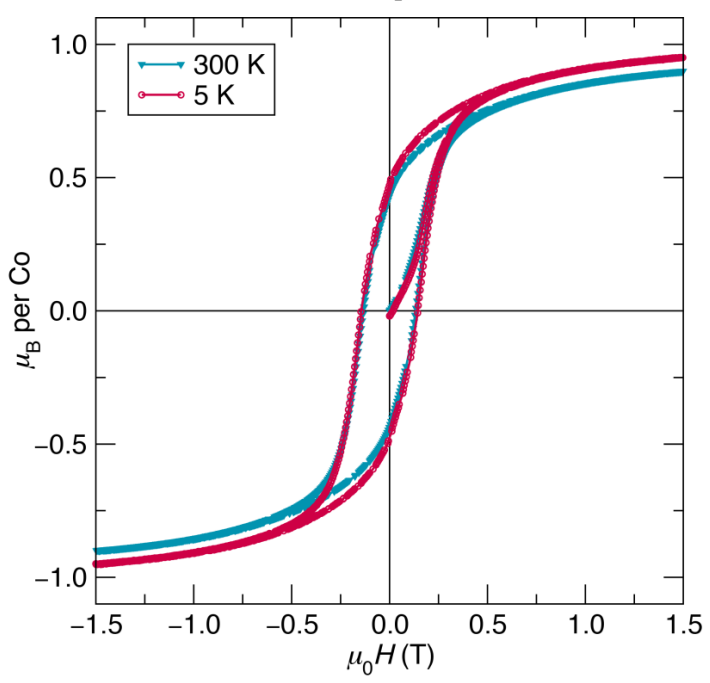


Figure 3: Magnetization as a function of magnetic field hysteresis loops for nanoparticles of Co_3B at 300 K and 5 K, showing semi-hard magnetic behavior.

The high-temperature properties of the nanoparticles of Co₃B are shown in Figure 4. The samples show a magnetic Curie temperature of about 710 K and a blocking temperature of 695 K, as determined from the maximum of the zero field-cooled magnetization. The observed Curie temperature is lower than that of the bulk material (750 K).³⁹ Again, this reduction compared to the bulk properties is often observed in nanoparticles, and was attributed to disorder at the nanoparticle surface. 47,55 Above the Curie temperature, however, a substantial magnetization signal is seen to persist, suggesting the presence of metallic cobalt ($T_c = 1400 \text{ K}$). This cobalt appears to form during the high-temperature experiment, because a comparison of room temperature M(H) before and after the experiment shows that the saturated moment increased over the course of the experiment, which involved heating to $T_{\text{max}} = 750 \text{ K}$ three times. Such an increase in moment would be expected with the partial decomposition of the Co₃B sample into Co₂B $(0.72 \mu_B/\text{Co})^{46}$ and Co $(1.7 \mu_B/\text{Co})^{56}$. In fact, in another attempt at high-temperature magnetic measurement where more time was spent at elevated temperature and the maximum temperature was higher (up to 773 K), M(H) at room temperature after the experiment showed a saturation magnetization of 1.2 μ_B /Co (see Supporting Information, Figure S3), which is larger than the fully saturated low-temperature moment of bulk Co₃B, indicating that the observed changes in magnetization cannot simply be the result of increased particle size or improved crystallinity of the Co₃B phase. Figure 4 (c) shows the sample decomposition in situ, as measured magnetization increases over time as the sample is held at 773 K. An increase of 8 % in measured moment is observed over the course of 10 minutes.

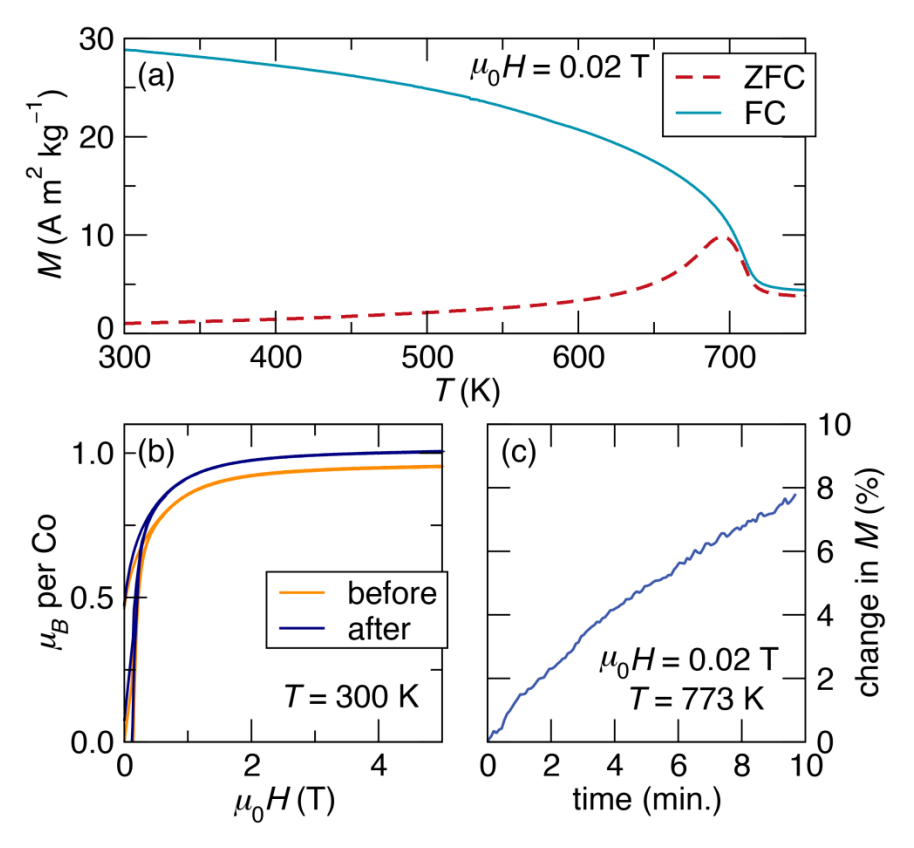


Figure 4: Magnetization properties of Co₃B nanoparticles at high temperature. (a) Magnetization as a function of temperature, collected upon warming under a 0.02 T field, either after cooling in zero field

(ZFC) or after cooling in the 0.02 T field (FC). During this measurement, some decomposition of the sample occurred, as evidenced by an increased room temperature saturation magnetization after the experiment (b). (c) When the sample was held at 773 K, the moment increased with time as the sample decomposed.

Due to the fact that Co₂B had already proven its catalytic activity in the oxygen evolution reaction (OER) in the past, ^{2,7,12,57,58} the investigation of the electrochemical performance of single-phase crystalline nanoparticles of Co₃B in the water splitting reaction was highly promising. The X-ray diffraction data after storing the particles in air at room temperature for two months showed no signs of decomposition or oxidation (see Supporting Information, Figure S4). XPS measurements were conducted before and after the electrochemical investigation (EC) of the powders to evaluate changes in the electronic structure and oxidation state during the electrochemical reaction. The Co 2p photoemission line of the sample after exposure to air is shown in Figure 5(a). The main peak of the Co 2p^{3/2} photoemission line is located at around 781.2 eV, while a broad satellite structure is visible at higher binding energies.

This structure indicates a strong oxidation of the surface of the Co₃B nanoparticles, where Co is found mostly in a 2+ oxidation state. The photoemission lines of oxygen and boron are shown in Figure 5(b) and (c), respectively. The B 1s detail spectrum shows only one component of oxidized boron (BO_x) at a binding energy of around 192.3 eV. In literature, the oxidized boron species can be found around 193.8 eV. However, in more recent studies of oxidized metal borides the binding energies of the B 1s photoemission lines were recorded at slightly lower binding energies around 192 to 193 eV compared to B1s photoemission lines in boron oxide, highly lower binding energies around 192 to 193 eV compared to B1s photoemission lines in boron oxide, which can be explained by the metal ions present in borates, leading to a slightly more negative charge at the boron. From these observations it is evident that the Co₃B nanoparticles were oxidized to a certain degree, while the bulk phase remains in the Co₃B state.

This development of a core-shell structure has been found before for nanostructured metal borides. 2,7,63 The O 1s detail spectrum (Figure 5b) is fitted based on the boron and cobalt components with a Shirley background and a mixed Gaussian-Lorentz peak shape and an oxocarbon species at higher binding energies ($\approx 533.8 \text{ eV}$). Due to the position of the cobalt species at around 531.3 eV, it can be concluded that cobalt forms a hydroxide (Co(OH)₂) at the surface. $^{59-61}$ The B-O bonding (BO_x) can be found at slightly higher binding energies around 532.3 eV. 62,64,65

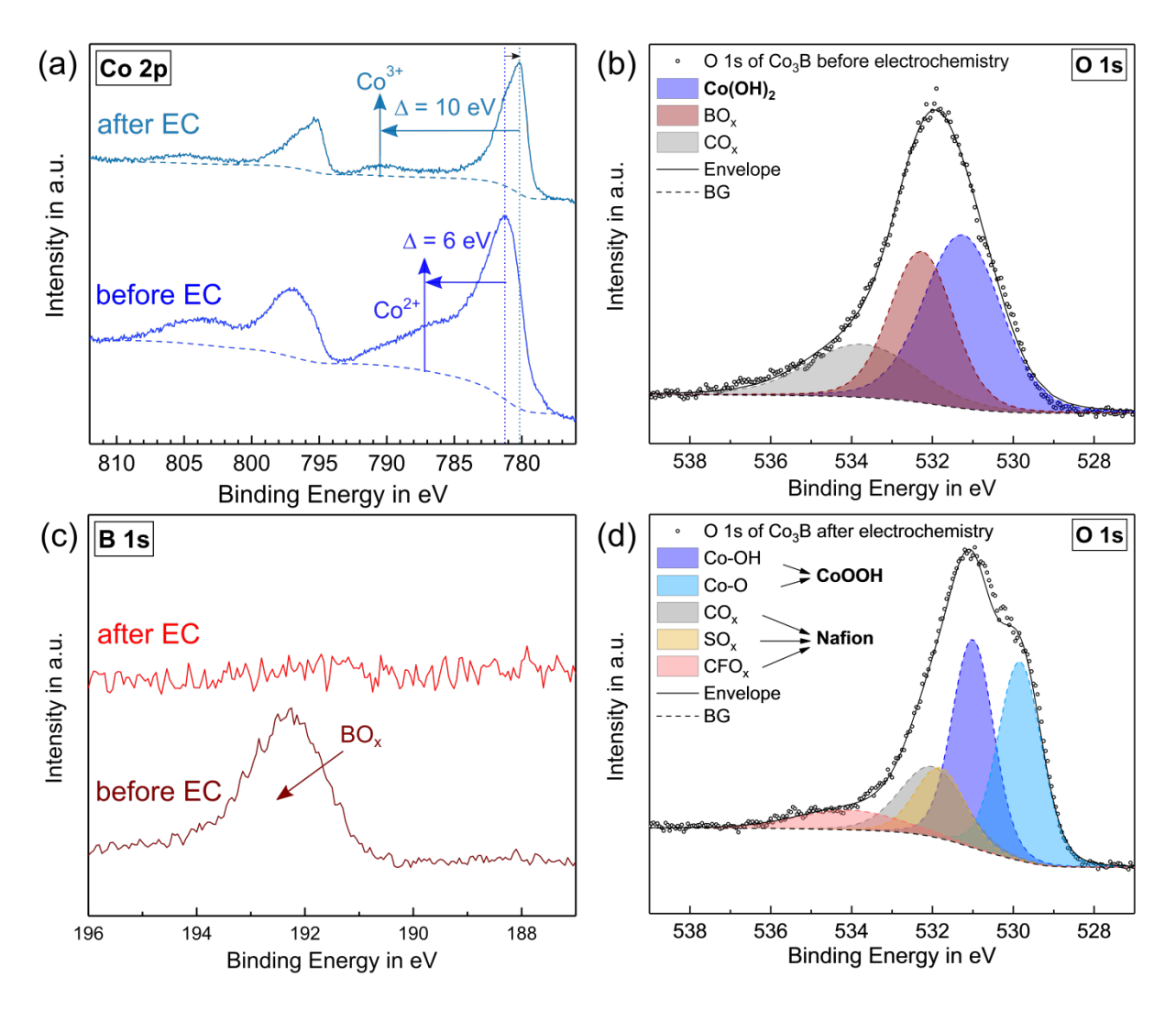


Figure 5: XP detail spectra of the Co₃B catalyst, before and after the electrochemical testing. (a) Co 2p and (c) B 1s spectra before and after the EC procedure. (b) and (d) fitted O 1s spectrum of the Co₃B catalyst before and after EC testing, respectively.

The electrochemical behavior of Co_3B was investigated in 1 M KOH, using glassy carbon as the substrate material. The electrocatalysts were first activated by cycling between 1 and 1.5 V vs. RHE (Figure S5), before measuring the catalytic activity. The CV curves of Co_3B after this activation procedure are shown in Figure 6a. They exhibit a broad hysteresis between 1.0 and 1.55 V, indicating oxidation and reduction reactions of the catalyst material. The width of the hysteresis highlights the high active surface area of the nanoparticles. Compared to Co_2B , which was previously characterized in our group, 7 the Co_3B catalyst shows an improved onset potential around 1.55 V vs. RHE. Additionally, the overpotential is strongly reduced from $\eta = 430 \text{ mV}^7$ to $\eta = 350 \text{ mV}$ at 20 mA cm⁻². Other studies on cobalt borides showed an overpotential of $\eta = 380 \text{ mV}$ in 0.1 M KOH² and $\eta = 345 \text{ mV}$ in 1 M KOH at 10 mA cm⁻². Second in the performance of different metal borides can be found in the Supporting Information (Table S1). According to these first electrochemical measurements, Co_3B seems to be a promising candidate for more detailed OER investigations. As shown in our previous study, 7 the performance of Co_3B may be further improved by incorporation of iron into this nanoscale boride.

However, Co₃B shows no bi-functional catalytic behavior for the water splitting reaction, since the activity in the HER is, in contrast to the OER activity, significantly lower (Figure 6b). This is surprising, since catalytic activity of other cobalt borides in HER has been reported.^{16,18}

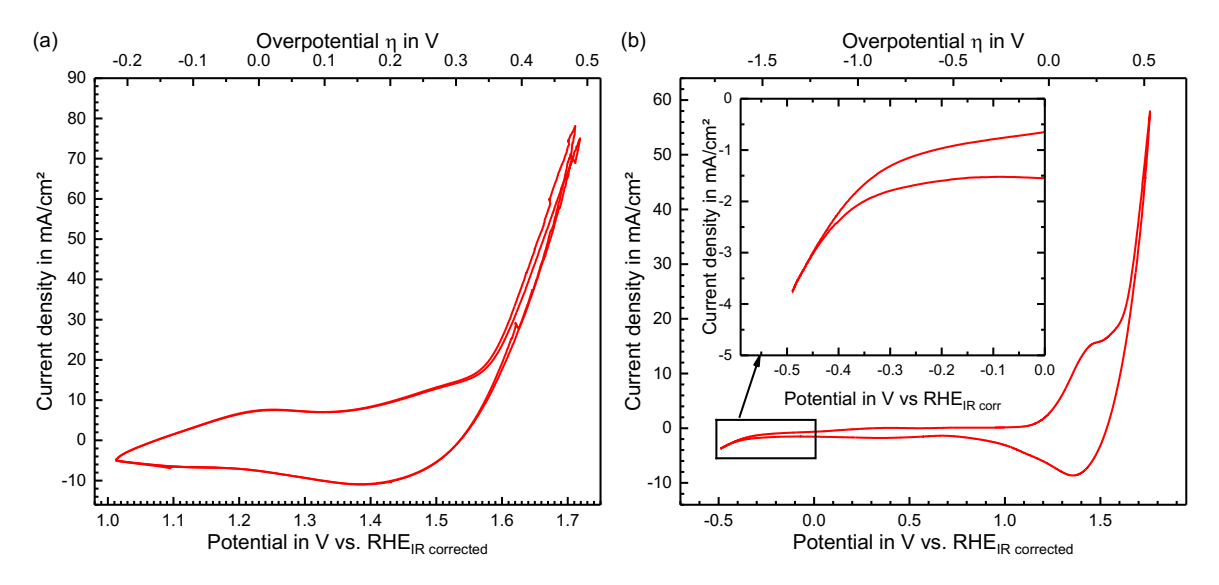


Figure 6: Electrochemical measurements in 1 M KOH. CV curves of Co_3B during the oxygen evolution reaction (a) with a scan rate of 10 mV s⁻¹ and (b) over the whole water splitting range with a scan rate of 50 mV s⁻¹ (inset gives a more detailed view on the HER). The potential is plotted versus the reversible hydrogen electrode (RHE) and is iR compensated.

XPS analysis of the surface was additionally performed after the electrochemical testing of the Co₃B catalyst, in order to observe changes of the catalytically active species at the surface introduced by redox reactions during the electrochemical measurement. The survey spectra before and after EC are shown in Figure S6. Figure 5(a) shows the Co 2p photoemission line after the electrochemical investigation. The Co 2p^{3/2} signal previously assigned to Co²⁺ was shifted to lower binding energies at around 780.2 eV, which indicates a change in oxidation state from Co²⁺ to Co³⁺. Additionally, the satellite of the Co 2p^{3/2} was shifted to higher binding energies, increasing the Co 2p^{3/2} to satellite distance from about 6 eV before to about 10 eV (790.2 eV) after the electrochemical testing, which is characteristic for the Co³⁺ species.^{7,59-61} This observation is further confirmed by the O 1s photoemission line shown in Figure 5d. The former hydroxide component in Co²⁺(OH)₂ found before the electrochemical testing is transformed into one oxide (529.8 eV) and one hydroxide (531.50 eV) component due to the formation of Co³⁺OOH, ⁶⁶⁻⁶⁸ which is in agreement with several other studies concerning cobalt-based OER catalysts. ^{2,66,69-72} The hydroxide signal seems to be more pronounced than the oxide one, which can be explained by the sulfone (SO_2 -OH – 531.8 eV) and oxocarbon (CO_x – 532.1 eV) components of the Nafion binder overlapping with the cobalt hydroxide signal. After the electrochemical testing the boron signal disappeared completely. Identical phenomena have been observed for metal borides in catalysis before. ^{2,5,7,57,63} The core-shell structure of our particles arises through an initial oxidation of the metal boride in air, followed by a stronger oxidation during the electrochemical treatment in an aqueous electrolyte, which leads to the formation of CoOOH at the surface, while the bulk or rather the core of the boride grains stays intact. Here, the surface shell of CoOOH most likely functions as the catalytically active phase, and the core of Co_3B possesses a higher conductivity than the shell structure 1,63,73 and therefore improves the overall performance of the catalyst.

Conclusion

In this work, we obtained phase-pure nanoparticles of metastable Co₃B nanoparticles for the first time by using a low-temperature solution synthesis procedure. Rinsing the precipitate with ethanol before briefly annealing at 773 K proved to be essential to obtain phase-pure samples. Synchrotron X-ray powder diffraction and TEM investigations confirmed that the particles were phase-pure, with particles sizes around 11 nm to 22 nm. Magnetic measurements showed a Curie temperature ($T_c = 710 \text{ K}$) and saturation magnetization at 5 K ($M_S = 1.02 \mu_B/\text{Co}$) slightly lower than described for the bulk material, as expected for nanoparticles. Magnetic hysteresis was observed, indicating that the semi-hard magnetic properties of Co₃B are retained in the nanoscale. We observed thermal decomposition during magnetic measurements at 750 K. In the oxygen evolution reaction, the Co₃B nanoparticles showed a low onset potential of 1.55 V vs. RHE. Although XRD results in reflections of only Co₃B after exposure to air, XPS revealed the formation of Co²⁺ and oxidized boron at the surface. During the electrochemical measurements, this core-shell structure was further oxidized. XPS measurements showed CoOOH which is also believed to be the catalytically active species for the oxygen evolution reaction. Due to their phase-purity, high magnetic moment, magnetic coercivity, and catalytic properties, these particles are promising for catalytic and magnetic applications.

Supporting Information: Particle size distribution of Co_3B after annealing at 773 K, effect of annealing temperature on the composition of the cobalt boride samples, room temperature M(H) after heating to 773 K, evaluation of air stability of Co_3B nanoparticles, electrochemical conditioning of the Co_3B nanoparticles, XPS survey spectra, comparison of the catalytic activity of different metal borides for the OER, Crystallographic Information File (.cif) of the refined Co_3B structure.

AUTHOR INFORMATION

Corresponding Authors

- *¹ Prof. Dr. Barbara Albert, Technische Universität Darmstadt, Eduard-Zintl-Institute of Inorganic and Physical Chemistry, Alarich-Weiss-Str. 12, 64287 Darmstadt, Germany, albert@ac.chemie.tu-darmstadt.de
- *2 Prof. Dr. Ram Seshadri, University of California, Santa Barbara, Department of Chemistry & Biochemistry, Materials Department, and Materials Research Laboratory, University of California, Santa Barbara CA 93106, U.S.A., seshadri@mrl.ucsb.edu

ACKNOWLEDGEMENTS

The authors acknowledge financial support by the DFG in the framework of the Darmstadt Graduate School of Excellence for Energy Science and Engineering (GSC1070). The transmission electron microscopes used in this work were partially funded by the German Research Foundation (DFG/INST163/2951). The work at UC Santa Barbara was supported by the National Science Foundation (NSF) through DMR 1710638. J.D.B. is supported by the NSF Graduate Research Fellowship Program under Grant No. 1650114. The use of shared experimental facilities of the NSF Materials Research Science and Engineering Center (MRSEC) at UC Santa Barbara under DMR 1720256 is gratefully acknowledged; the UC Santa Barbara MRSEC is a member of the NSF-supported Materials Research Facilities Network (www.mrfn.org). Use of the Advanced Photon Source at Argonne National Laboratory was supported by the U.S. Department of Energy, Office of Science, Office of Basic Energy Sciences, under Contract No. DE-AC02-06CH11357. We thank the 11-BM staff for their assistance with the data collection. The authors would like to thank Dr. Stefan Lauterbach and Stephanie Dolique for help with the TEM investigations.

REFERENCES

- (1) Carenco, S.; Portehault, D.; Boissière, C.; Mézailles, N.; Sanchez, C. Nanoscaled Metal Borides and Phosphides: Recent Developments and Perspectives. *Chem. Rev.* **2013**, *113*, 7981-8065.
- (2) Masa, J.; Weide, P.; Peeters, D.; Sinev, I.; Xia, W.; Sun, Z.; Somsen, C.; Muhler, M.; Schuhmann, W. Amorphous Cobalt Boride (Co₂B) as Highly Efficient Nonprecious Catalyst for Electrochemical Water Splitting: Oxygen and Hydrogen Evolution. *Adv. Energy Mater.* **2016**, *6*, 1502313.
- (3) Masa, J.; Sinev, I.; Mistry, H.; Ventosa, E.; de la Mata, M.; Arbiol, J.; Muhler, M.; Roldan Cuenya, B.; Schuhmann, W. Ultrathin High Surface Area Nickel Boride (Ni_xB) Nanosheets as Highly Efficient Electrocatalyst for Oxygen Evolution. *Adv. Energy Mater.* **2017**, *7*, 1700381.
- (4) Masa, J.; Andronescu, C.; Antoni, H.; Sinev, I.; Seisel, S.; Elumeeva, K.; Barwe, S.; Marti-Sanchez, S.; Arbiol, J.; Roldan Cuenya, B.; Muhler, M.; Schuhmann, W. Role of Boron and Phosphorous in Enhanced Electrocatalytic Oxygen Evolution by Nickel Borides and Nickel Phosphides. *ChemElectroChem* **2019**, *6*, 235-240.
- (5) Nsanzimana, J. M. V.; Peng, Y.; Xu, Y. Y.; Thia, L.; Wang, C.; Xia, B. Y.; Wang, X. An Efficient and Earth-Abundant Oxygen-Evolving Electrocatalyst Based on Amorphous Metal Borides. *Adv. Energy Mater.* **2018**, *8*, 1701475.
- (6) Nsanzimana, J. M. V.; Dangol, R.; Reddu, V.; Duo, S.; Peng, Y.; Dinh, K. N.; Huang, Z.; Yan, Q.; Wang, X. Facile Synthesis of Amorphous Ternary Metal Borides Reduced Graphene Oxide Hybrid with Superior Oxygen Evolution Activity *ACS Appl. Mater. Interfaces* **2019**, *11*, 846-855.
- (7) Klemenz, S.; Schuch, J.; Hawel, S.; Zieschang, A.-M.; Kaiser, B.; Jaegermann, W.; Albert, B. Synthesis of a Highly Efficient Oxygen-Evolution Electrocatalyst by Incorporation of Iron into Nanoscale Cobalt Borides. *ChemSusChem* **2018**, *11*, 3150-3156.
- (8) Jothi, P. R.; Zhang, Y.; Scheifers, J. P.; Park, H.; Fokwa, B. P. T. Molybdenum Diboride Nanoparticles as a Highly Efficient Electrocatalyst for the Hydrogen Evolution Reaction. *Sustainable Energy Fuels* **2017**, *1*, 1928-1934.

- (9) Park, H.; Encinas, A.; Scheifers, J. P.; Zhang, Y.; Fokwa, B. P. T. Boron-Dependency of Molybdenum Boride Electrocatalysts for the Hydrogen Evolution Reaction. *Angew. Chem. Int. Ed.* **2017**, *56*, 5575-5578.
- (10) Jiang, W.-J.; Niu, S.; Tang, T.; Zhang, Q.-H.; Liu, X.-Z.; Zhang, Y.; Chen, Y.-Y.; Li, J.-H.; Gu, L.; Wan, L.-J.; Hu, J.-S. Crystallinity-Modulated Electrocatalytic Activity of a Nickel(II) Borate Thin Layer on Ni₃B for Efficient Water Oxidation. *Angew. Chem. Int. Ed.* **2017**, *56*, 6572-6577.
- (11) Chen, Y.; Yu, G.; Chen, W.; Liu, Y.; Li, G.-D.; Zhu, P.; Tao, Q.; Li, Q.; Liu, J.; Shen. X.; Li, H.; Huang, X.; Wang, D.; Asefa, T. Zou, X. Highly Active, Nonprecious Electrocatalyst Comprising Borophene Subunits for the Hydrogen Evolution Reaction. *J. Am. Chem. Soc.* **2017**, *139*, 12370-12373.
- (12) Chen, H.; Ouyang, S.; Zhao, M.; Li, Y.; Ye, J. Synergistic Activity of Co and Fe in Amorphous Cox-Fe-B Catalyst for Efficient Oxygen Evolution Reaction. *ACS Appl. Mater. Interfaces* **2017**, *9*, 40333-40343.
- (13) Li, L.; Deng, Z.; Yu, L.; Lin, Z.; Wang, W.; Yang, G. Amorphous Transitional Metal Borides as Substitutes for Pt Cocatalysts for Photocatalytic Water Splitting. *Nano Energy* **2016**, *27*, 103-113.
- (14) Sun, H.; Meng, J.; Jiao, L.; Cheng, F.; Chen, J. A Review of Transition-metal Boride/Phosphide Based Materials for Catalytic Hydrogen Generation from Hydrolysis of Boron-Hydrides. *Inorg. Chem. Front.* **2018**, *5*, 760-772.
- (15) Xu, N.; Cao, G.; Chen, Z.; Kang, Q.; Dai, H.; Wang, P. Cobalt nickel boride as an active electrocatalyst for water splitting. *J. Mater. Chem. A* **2017**, *5*, 12379-12384.
- (16) Gupta, S.; Patel, N.; Fernandes, R.; Hanchate, S.; Miotello, A.; Kothari, D. C. Co-Mo-B Nanoparticles as non-precious and efficient Bifunctional Electrocatalyst for Hydrogen and Oxygen Evolution. *Elechtrochim. Acta* **2017**, *232*, 64-71.
- (17) Elumeeva, K.; Masa, J.; Medina, D.; Ventosa, E.; Seisel, S.; Kayran, Y. U.; Genç, A.; Bobrowski, T.; Weide, P.; Arbiol, J.; Muhler, M.; Schuhmann, W. Cobalt Boride Modified with N-doped Carbon Nanotubes as a High-performance Bifunctional Oxygen Electrocatalyst. *J. Mater. Chem. A* **2017**, *5*, 21122-21129.
- (18) Gupta, S.; Patel, N.; Miotello, A.; Kothari, D. C. Cobalt-Boride: An efficient and robust electrocatalyst for Hydrogen Evolution Reaction. *J. Power Sources* **2015**, *279*, 620-625.
- (19) Kalyon, N.; Hofmann, K.; Malter, J.; Lucas, M.; Claus, P.; Albert, B. Catalytic Activity of Nanoscale Borides: Co₂B and Ni₇B₃ in the Liquid-phase Hydrogenation of Citral. *J. Catal.* **2017**, *352*, 436-441.
- (20) Wu, C.; Wu, F.; Bai, Y.; Yi, B.; Zhang, H. Cobalt Boride Catalysts for Hydrogen Generation from Alkaline NaBH₄ solution. *Mater. Lett.* **2005**, *59*, 1748-1751.
- (21) Li, H.; Li, H.; Wang, M. Glucose Hydrogenation over Promoted Co-B amorphous alloy catalysts. *Appl. Catal., A* **2001**, *207*, 129-137.

- (22) Li, H.; Chen, X.; Wang, M.; Xu, Y. Selective Hydrogenation of Cinnamaldehyde to Cinnamyl Alcohol over an Ultrafine Co-B Amorphous Alloy Catalyst. *Appl. Catal.*, *A* **2002**, *225*, 117-130.
- (23) Hofmann, K.; Kalyon, N.; Kapfenberger, C.; Lamontagne, L.; Zarrini, S.; Berger, R.; Seshadri, R.; Albert, B. Metastable Ni₇B₃: A New Paramagnetic Boride from Solution Chemistry, Its Crystal Structure and Magnetic Properties. *Inorg. Chem.* **2015**, *54*, 10873-10877.
- (24) Kapfenberger, C.; Hofmann, K.; Albert, B. Room-temperature Synthesis of Metal Borides. *Solid State Sci.* **2003**, *5*, 925-930.
- (25) Glavee, G. N.; Klabunde, K. J.; Sorensen, C. M.; Hadjipanayis, G. C. Borohydride Reductions of Metal Ions. A New Understanding of the Chemistry Leading to Nanoscale Particles of Metals, Borides, and Metal Borates. *Langmuir* **1992**, *8*, 771-773.
- (26) Glavee, G. N.; Klabunde, K. J.; Sorensen, C. M.; Hadjipanayis, G. C. Borohydride Reduction of Cobalt Ions in Water. Chemistry Leading to Nanoscale Metal, Boride, or Borate Particles. *Langmuir* **1993**, *9*, 162-169.
- (27) Glavee, G. N.; Klabunde, K. J.; Sorensen, C. M.; Hadjipanayis, G. C. Chemistry of Borohydride Reduction of Iron(II) and Iron(III) Ions in Aqueous and Nonaqueous Media. Formation of Nanoscale Fe, FeB, and Fe₂B Powders. *Inorg. Chem.* **1995**, *34*, 28-35.
- (28) Demirci, U. B.; Miele, P. Cobalt in NaBH₄ Hydrolysis. *Phys. Chem. Chem. Phys.* **2010**, *12*, 14651-14665.
- (29) Schlesinger, H. I.; Brown, H. C.; Finholt, A. E.; Gilbreath, J. R.; Hoekstra, H. R.; Hyde, E. K. Sodium Borohydride, Its Hydrolysis and its Use as a Reducing Agent and in the Generation of Hydrogen. *J. Am Chem. Soc.* **1953**, *75*, 215-219.
- (30) Rades, S.; Kraemer, S.; Seshadri, R.; Albert, B. Size and Crystallinity Dependence of Magnetism in Nanoscale Iron Boride, α-FeB. *Chem. Mater.* **2014**, *26*, 1549-1552.
- (31) Yiping, L.; Hadjipanayis, G. C.; Sorensen, C. M.; Klabunde, K. J. Magnetic and Structural Properties of Ultrafine Co-B Particles. *J. Magn. Magn. Mater.* **1989**, *79*, 321-326.
- (32) Portehault, D.; Devi, S.; Beaunier, P.; Gervais, C.; Giordano, C.; Sanchez, C.; Antonietti, M. A General Solution Route toward Metal Boride Nanocrystals. *Angew. Chem. Int. Ed.* **2011**, *50*, 3262-3265.
- (33) Gouget, G.; Debecker, D. P.; Kim, A.; Olivieri, G.; Gallet, J.-J.; Bournel, F.; Thomas, C.; Ersen, O.; Moldovan, S.; Snachez, C.; Carenco, S.; Portehault, D. In Situ Solid-Gas Reactivity of Nanoscaled Metal Borides from Molten Salt Synthesis. *Inorg. Chem.* **2017**, *56*, 9225-9234.
- (34) Jothi, P. R.; Yubuta, K.; Fokwa, B. P. T. A Simple, General Synthetic Route toward Nanoscale Transition Metal Borides. *Adv. Mater.* **2018**, *30*, 1704181.
- (35) Corrias, A.; Ennas, G.; Licheri, G.; Marongiu, G.; Paschina, G. Amorphous Metallic Powders Prepared by Chemical Reduction of Metal Ions with Potassium Borohydride in Aqueous Solution. *Chem. Mater.* **1990**, *2*, 363-366.

- (36) Lefterova, E.; Dragieva, I.; Tchanev, V.; Mehandjiev, D.; Mikhov, M. Crystallographic phases in nanosized ferromagnetic particles obtained by two different methods. *J. Magn. Magn. Mater.* **1995**, *140-144*, 457-458.
- (37) Rundqvist, S. Crystal Structure of Ni₃B and Co₃B. Acta Chem. Scand. 1958, 12, 658-662.
- (38) Omori, S.; Hashimoto, Y. Eutectoid Decomposition of Co₃B and Phase Diagram of the System Co-Co₂B. *Trans. Jpn. Inst. Met.* **1976**, *17*, 571-574.
- (39) Pal, S. K.; Skokov, K. P.; Groeb, T.; Ener, S.; Gutfleisch, O. Properties of Magnetically Semihard (Fe_xCo_{1-x})₃B Compounds. *J. Alloys Compd.* **2017**, *696*, 543-547.
- (40) Ma, X.; Wen, J.; Zhang, S.; Yuan, H.; Li, K.; Yan, F.; Zhang, X.; Chen, Y. Crystal Co_xB (x = 1-
- 3) Synthesized by a Ball-Milling Method as High-Performance Electrocatalysts for the Oxygen Evolution Reaction. *ACS Sustainable Chem. Eng.* **2017**, *5*, 10266-10274.
- (41) Bratz, K.; Wörz, N.; Brandner, A.; Hofmann, K.; Claus, P.; Albert, B. Co₂B als interessanter Katalysator in der Citralhydrierung. *Z. Anorg. Allg. Chem.* **2010**, *636*, 2098.
- (42) Wang, Y. D.; Ai, X. P.; Cao, Y. L.; Yang, H. X. Exceptional electrochemical activities of amorphous Fe-B and Co-B alloy powders used as high capacity anode materials. *Electrochem. Commun.* **2004**, *6*, 780-784.
- (43) Grant, J. T.; McDermott, W. P.; Venegas, J. M.; Burt, S. P.; Micka, J.; Phivilay, S. P.; Carrero, C. A.; Hermans, I. Boron and Boron-Containing Catalysts for the Oxidative Dehydrogenation of Propane. *ChemCatChem* **2017**, *9*, 3623-3626.
- (44) Bocarsly, J. D.; Levin, E. E.; Humphrey, S. A.; Faske, T.; Donner, W.; Wilson, S. D.; Seshadri, R. Magnetostructural Coupling Drives Magnetocaloric Behavior: The Case of MnB versus FeB. *Chem. Mater.* **2019**, *31*, 4873.
- (45) Gutfleisch, O.; Willard, M. A.; Brück, E.; Chen, C. H.; Sankar, S. G.; Liu, J. P. Magnetic Materials and Devices for the 21st Century: Stronger, Lighter, and More Energy Efficient. *Adv. Mater.* **2011**, *23*, 821-842.
- (46) Edström, O.; Werwiński M.; Iuşan, D.; Rusz, J.; Eriksson, O.; Skokov, K. P.; Radulov, I. A.; Ener, S.; Kuz'min, M. D.; Hong, J.; Fries, M.; Karpenkov, D. Y.; Gutfleisch, O.; Toson, P.; Fidler, J. Magnetic properties of (Fe_{1-x}Co_x)₂B alloys and the effect of doping by 5d elements. *Phys. Rev. B* **2015**, *92*, 174413.
- (47) Zieschang, A.-M.; Bocarsly, J. D.; Dürrschnabel, M.; Molina-Luna, L.; Kleebe, H.-J.; Seshadri, R.; Albert, B. Nanoscale Iron Nitride, ε-Fe₃N: Preparation from Liquid Ammonia and Magnetic Properties. *Chem. Mater.* **2017**, *29*, 621-628.
- (48) Zieschang, A.-M.; Bocarsly, J. D.; Dürrschnabel, M.; Kleebe, H.-J.; Seshadri, R.; Albert, B. Low-Temperature Synthesis and Magnetostructural Transition in Antiferromagnetic, Refractory Nanoparticles: Chromium Nitride, CrN. *Chem. Mater.* **2018**, *30*, 1610-1616.
- (49) Iga, A. Magneto-Crystalline Anisotropy of Co₂B. J. Phys. Soc. Japan 1966, 21, 1464.
- (50) Iga, A. Magnetocrystalline Anisotropy of Fe₂B. J. Phys. Soc. Japan 1966, 21, 404.

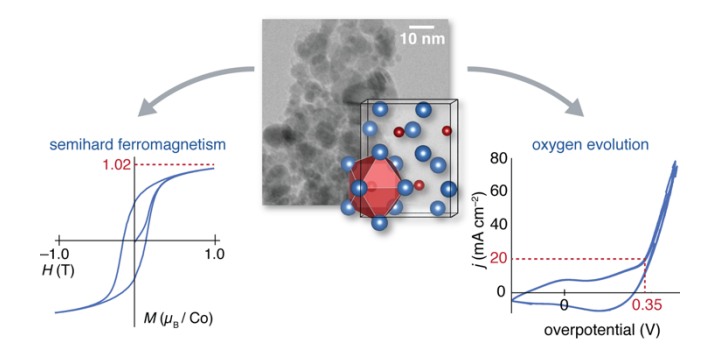
- (51) Iga, A. Magnetocrystalline Anisotropy in (Fe_{1-x}Co_x)₂B System. *Japan. J. Appl. Phys.* **1970**, 9, 415-416.
- (52) Stephens, P. W. Phenomenological model of anisotropic peak broadening in powder diffraction. *J. Appl. Cryst.* **1999**, *32*, 281-289.
- (53) Fruchart, D.; Chaudouet, P.; Fruchart, R.; Rouault, A., Senateur, J. P. Etudes structurales de composés de type cémentite: Effet de l'hydrogène sur Fe₃C suivi par diffraction neutronique. Spectrométrie Mössbauer sur FeCo₂B et Co₃B dopés au ⁵⁷Fe. *J. Solid State Chem.* **1984**, *51*, 246-252.
- (54) Fruchart, R., Moments magnétiques des borures ferromagnétiques de cobalt Co₃B, Co₂B et du borure de fer FeB. C. R. Hebd. Seances Acad. Sci. 1963, 256, 3304-3305.
- (55) Lu, A.-H.; Salabas, E. L.; Schüth, F. Magnetic Nanoparticles: Synthesis, Protection, Functionalization, and Application. *Angew. Chem. Int. Ed.* **2007**, *46*, 1222-1244.
- (56) Childress, J. R.; Chien, C. L. Reentrant Magnetic Behavior in fcc Co-Cu Alloys. *Phys. Rev. B* **1991**, *10*, 8089-8093.
- (57) Zhang, J.; Li, X.; Liu, Y.; Zeng, Z.; Cheng, X.; Wang, Y.; Tu, W.; Pan, M. Bi-metallic boride electrocatalysts with enhanced activity for the oxygen evolution reaction. *Nanoscale* **2018**, *10*, 11997-12002.
- (58) Chen, P.; Xu, K.; Zhou, T.; Tong, Y.; Wu, J.; Cheng, H.; Lu, X.; Ding, H.; Wu, C.; Xie, Y. Strong-Coupled Cobalt Borate Nanosheets/Graphene Hybrid as Electrocatalyst for Water Oxidation Under Both Alkaline and Neutral Conditions. *Angew. Chem. Int. Ed.* **2016**, *55*, 2488-2492.
- (59) Yang, J.; Liu, H.; Martens, W. N.; Frost, R. L. Synthesis and Characterization of Cobalt Hydroxide, Cobalt Oxyhydroxide, and Cobalt Oxide Nanodiscs. *J. Phys. Chem. C* **2010**, *114*, 111-119.
- (60) Biesinger, M. C.; Payne, B. P.; Grosvenor, A. P.; Lau, L. W. M.; Gerson, A. R.; Smart, R. S. C. Resolving surface chemical states in XPS analysis of first row transition metals, oxides and hydroxides: Cr, Mn, Fe, Co and Ni. *Appl. Surf. Sci.* **2011**, *257*, 2717-2730.
- (61) Oku, M.; Hirokawa, K. X-ray photoelectron spectroscopy of Co₃O₄, Fe₃O₄, Mn₃O₄, and related compounds. *J. Electron Spectrosc. Relat. Phenom.* **1976**, *8*, 475-481.
- (62) Legrand, J.; Gota, S.; Guittet, M.-J.; Petit, C. Synthesis and XPS Characterization of Nickel Boride Nanoparticles. *Langmuir* **2002**, *18*, 4131-4137.
- (63) Shveikin, G. P.; Ivanovskii, A. L. The chemical bonding and electronic properties of metal borides. *Russ. Chem. Rev.***1994**, *63*, 711-734.
- (64) Wang, Y.; Fan, J.; Trenary, M. Surface chemistry of boron oxidation. 1. Reactions of oxygen and water with boron films grown on tantalum(110). *Chem. Mater.* **1993**, *5*, 192-198.
- (65) Wang, Y.; Trenary, M. Surface chemistry of boron oxidation. 2. The reactions of boron oxides B₂O₂ and B₂O₃ with boron films grown on tantalum(110). *Chem. Mater.* **1993**, *5*, 199-205.
- (66) Weidler, N.; Paulus, S.; Schuch, J.; Klett, J.; Hoch, S.; Stenner, P.; Malkusch, A.; Brötz, J.; Wittich, C.; Kaiser, B.; Jaegermann, W. CoO_x thin film deposited by CVD as efficient water oxidation

- catalyst: change of oxidation state in XPS and its correlation to electrochemical activity. *Phys. Chem. Chem. Phys.* **2016**, *18*, 10708-10718.
- (67) Yang, Y.; Fei, H.; Ruan, G.; Tour, J. M. Porous Cobalt-Based Thin Film as a Bifunctional Catalyst for Hydrogen Generation and Oxygen Generation. *Adv. Mater.* **2015**, *27*, 3175-3180.
- (68) McIntyre, N. S.; Cook, M. G. X-ray photoelectron studies on some oxides and hydroxides of cobalt, nickel, and copper. *Anal. Chem.* **1975**, *47*, 2208-2213.
- (69) Burke, M. S.; Kast, M. G.; Trotochaud, L.; Smith, A. M.; Boettcher, S. W. Cobalt-Iron (Oxy)hydroxide Oxygen Evolution Electrocatalysts: The Role of Structure and Composition on Activity, Stability and Mechanism. *J. Am. Chem. Soc.* **2015**, *137*, 3638-3648.
- (70) Burke, M. S.; Zou, S.; Enman, L. J.; Kellon, J. E.; Gabor, C. A.; Pledger, E.; Boettcher, S. W. Revised Oxygen Evolution Reaction Activity Trends for First-Row Transition-Metal (Oxy)hydroxides in Alkaline Media. *J. Phys. Chem. Lett.* **2015**, *6*, 3737-3742.
- (71) Trotochaud, L.; Boettcher, S. W. Precise oxygen evolution catalysts: Status and opportunities. *Scr. Mater.* **2014**, *74*, 25-32.
- (72) Subbaraman, R.; Tripkovic, D.; Chang, K.-C.; Strmcnik, D.; Paulikas, A. P.; Hirunsit, P.; Chan, M.; Greeley, J.; Stamenkovic, V.; Markovic, N. Trends in activity for the water electrolyser reactions on 3d M(Ni,Co,Fe,Mn) hydr(oxy)oxide catalysts. *Nat. Mater.* **2012**, *11*, 550-557.
- (73) Wang, C. C.; Akbar, S. A.; Chen, W.; Patton, V. D. Electrical properties of high-temperature oxides, borides, carbides, and nitrides. *J. Mater. Sci.* **1995**, *30*, 1627-1641.

Synopsis - For Table of Contents Only

The synthesis of single-phase metastable Co₃B nanoparticles was enabled using a precipitation method followed by a brief annealing step. These semi-hard ferromagnetic particles had a saturation magnetization of 91 A m² kg⁻¹ and coercive field of 0.14 T at 5 K. The evaluation of their activity as an electrocatalyst in the oxygen evolution reaction showed a low onset potential of 1.55 V vs. RHE.

TOC graphic – For Table of Contents Only



Supporting Information

Magnetic and Electrocatalytic Properties of Nanoscale Cobalt Boride, Co₃B

Anne-Marie Zieschang,¹ Joshua D. Bocarsly,² Jona Schuch,³ Christina V. Reichel,¹ Bernhard Kaiser,³ Wolfram Jaegermann,³ Ram Seshadri,*,² Barbara Albert*,¹

Corresponding Authors

*¹ Prof. Dr. Barbara Albert, Technische Universität Darmstadt, Eduard-Zintl-Institute of Inorganic and Physical Chemistry, Alarich-Weiss-Str. 12, 64287 Darmstadt, Germany, albert@ac.chemie.tu-darmstadt.de

*2 Prof. Dr. Ram Seshadri, University of California, Santa Barbara, Department of Chemistry & Biochemistry, Materials Department, and Materials Research Laboratory, University of California, Santa Barbara CA 93106, U.S.A., seshadri@mrl.ucsb.edu

¹ Eduard-Zintl-Institute of Inorganic and Physical Chemistry, Technische Universität Darmstadt, Alarich-Weiss-Str. 12, 64287 Darmstadt, Germany

² Department of Chemistry & Biochemistry, Materials Department, and Materials Research Laboratory, University of California, Santa Barbara, Santa Barbara California 93106, United States

³ Institute of Materials Science (Surface Science Division), Technische Universität Darmstadt, Jovanka-Bontschits-Str. 2, 64287 Darmstadt, Germany

1. Particle size distribution of Co₃B nanoparticles after annealing at 773 K

The particle size distribution of the Co₃B nanoparticles was determined by transmission electron microscopy. Figure S1 shows the particle size distribution for Co₃B after annealing at 773 K.

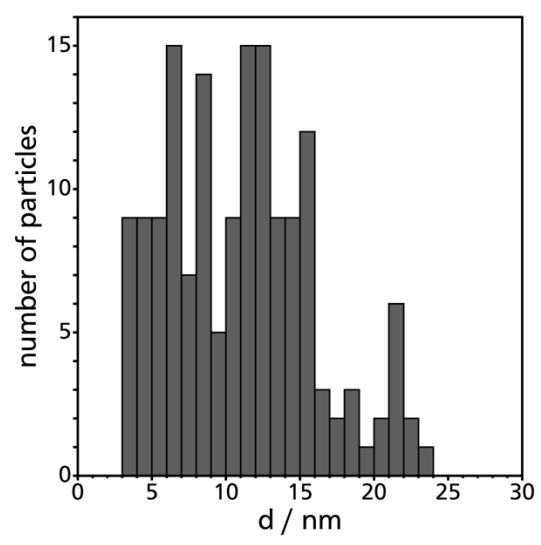


Figure S1: Particle size distribution of Co₃B after annealing at 773 K as determined by TEM.

2. Effect of annealing temperature on the composition of the cobalt boride samples

The samples were analyzed using X-ray diffraction after annealing at 773 K and 873 K. The results are shown in Figure S2. Two of the reflections of cobalt (Fm-3m) can be seen at 23.1 ° and 38.8 ° after annealing at 873 K (Figure S2 (b)).

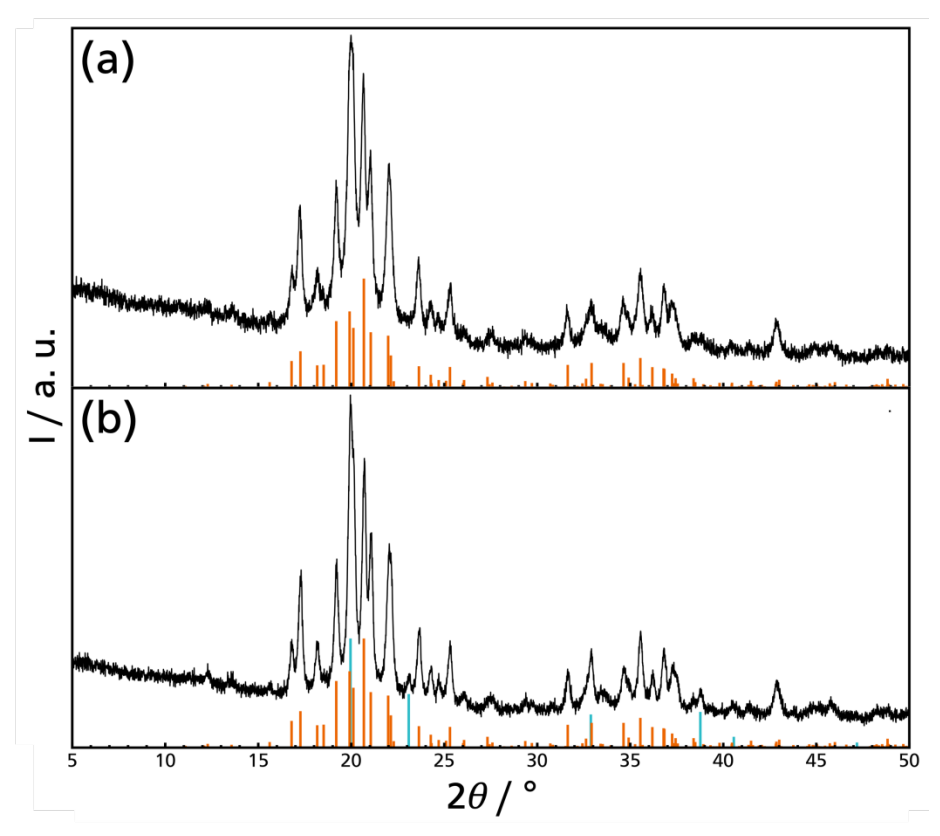


Figure S2: X-ray powder diffraction of the Co_3B nanoparticles after annealing at (a) 773 K and (b) 873 K compared to literature data of Co_3B (orange, *Pnma*, no. 603543)⁽¹⁾ and Co (blue, *Fm*-3*m*, no. 44989)⁽²⁾.

3. Room temperature M(H) after heating to 773 K

Magnetization as a function of magnetic field was collected for Co_3B nanoparticles before and after the high-temperature magnetization measurement which involved heating to 773 K (Figure S3). A saturation magnetization of 1.2 μ_B /Co after heating indicates the formation of a cobalt side phase during the experiment.

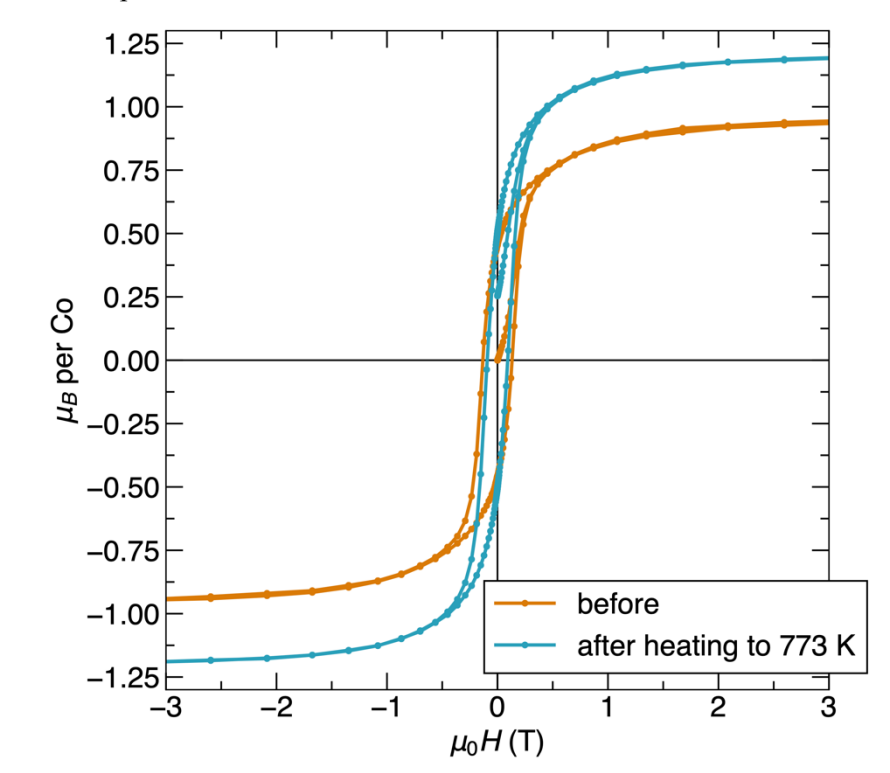


Figure S3: Comparison of the magnetization as a function of magnetic field for Co_3B nanoparticles at room temperature before and after heating to 773 K in the magnetometer.

4. Evaluation of air stability of Co₃B nanoparticles

After annealing at 773 K the Co₃B nanoparticles were stored in air at room temperature for two months. The X-ray diffraction data showed no change in the diffraction pattern (Figure S4).

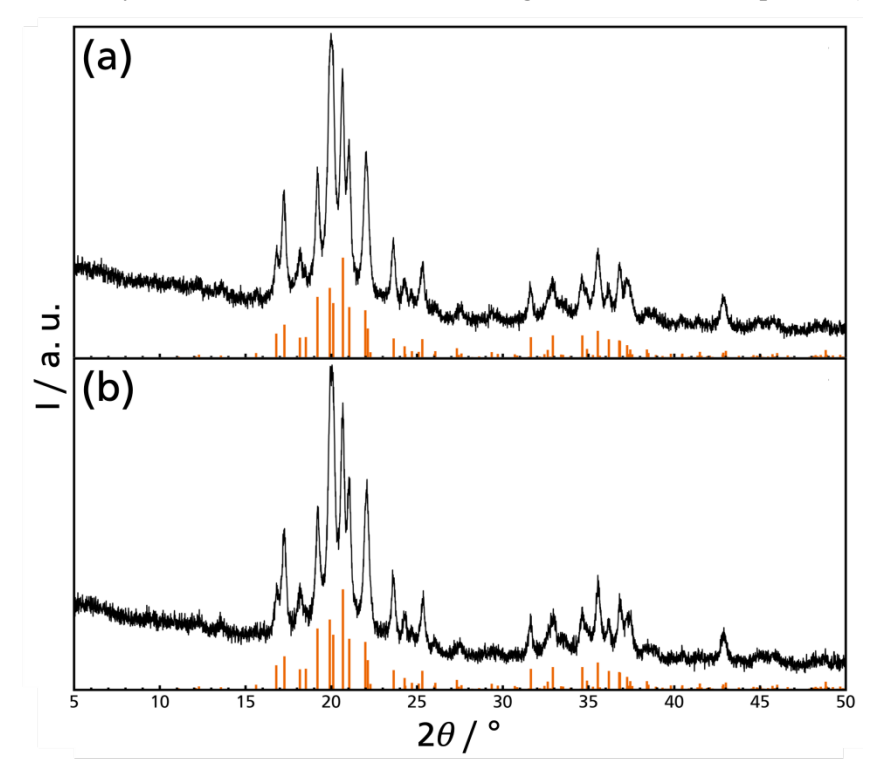


Figure S4: X-ray powder diffraction of the Co_3B nanoparticles after annealing at 773 K, (a) before and (b) after storage in air for two months compared to literature data of Co_3B (orange, Pnma, no. 603543)⁽¹⁾.

5. Electrochemical conditioning of the Co₃B nanoparticles

The activation procedure led to an oxidation of the catalyst. Two oxidation waves were visible, leading first to CoOOH (1.3 V vs. RHE) and possibly right before the start of the OER to Co^{4+} (around 1.5 V vs. RHE) at the surface. These oxidation waves have been investigated before in literature. However, the further oxidation to Co^{4+} is generally agreed on but has still not been demonstrated in literature in detail.⁽³⁾ Due to the reversible nature of the Co^{4+} oxidation state, the reduction wave was visible around 1.3 V vs. RHE (Co^{4+} to Co^{3+} oxidation state).

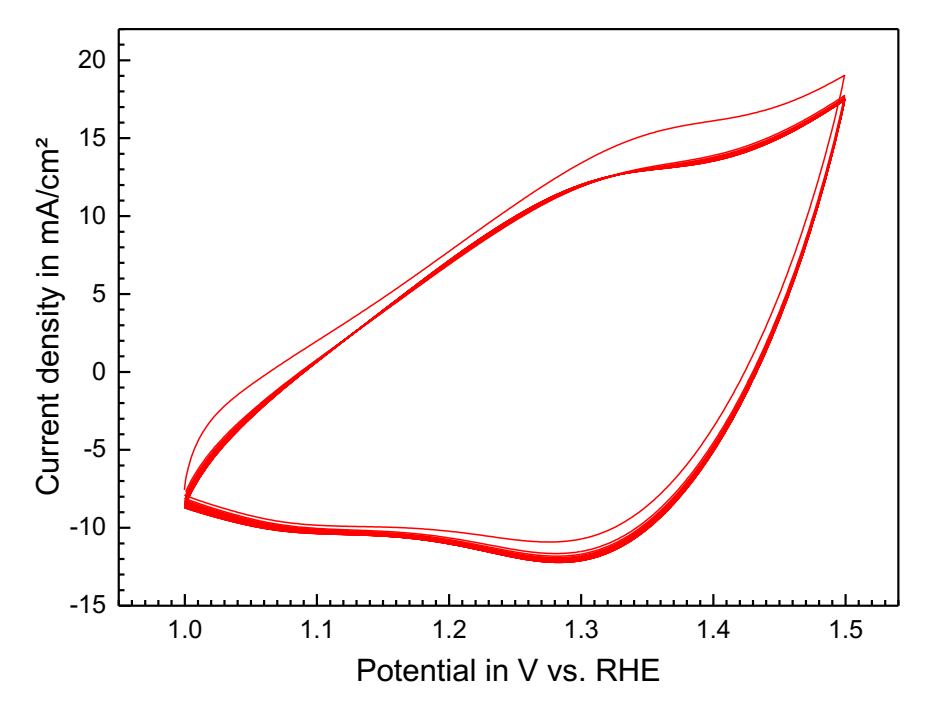


Figure S5: Electrochemical conditioning of the catalyst between 1 and 1.5 V vs. RHE using cyclic voltammetry in 1 M KOH with a scan rate of 100 mV/s for 30 cycles. Hg/HgO was used as a reference electrode and a Pt wire as counter electrode.

6. XPS survey spectra

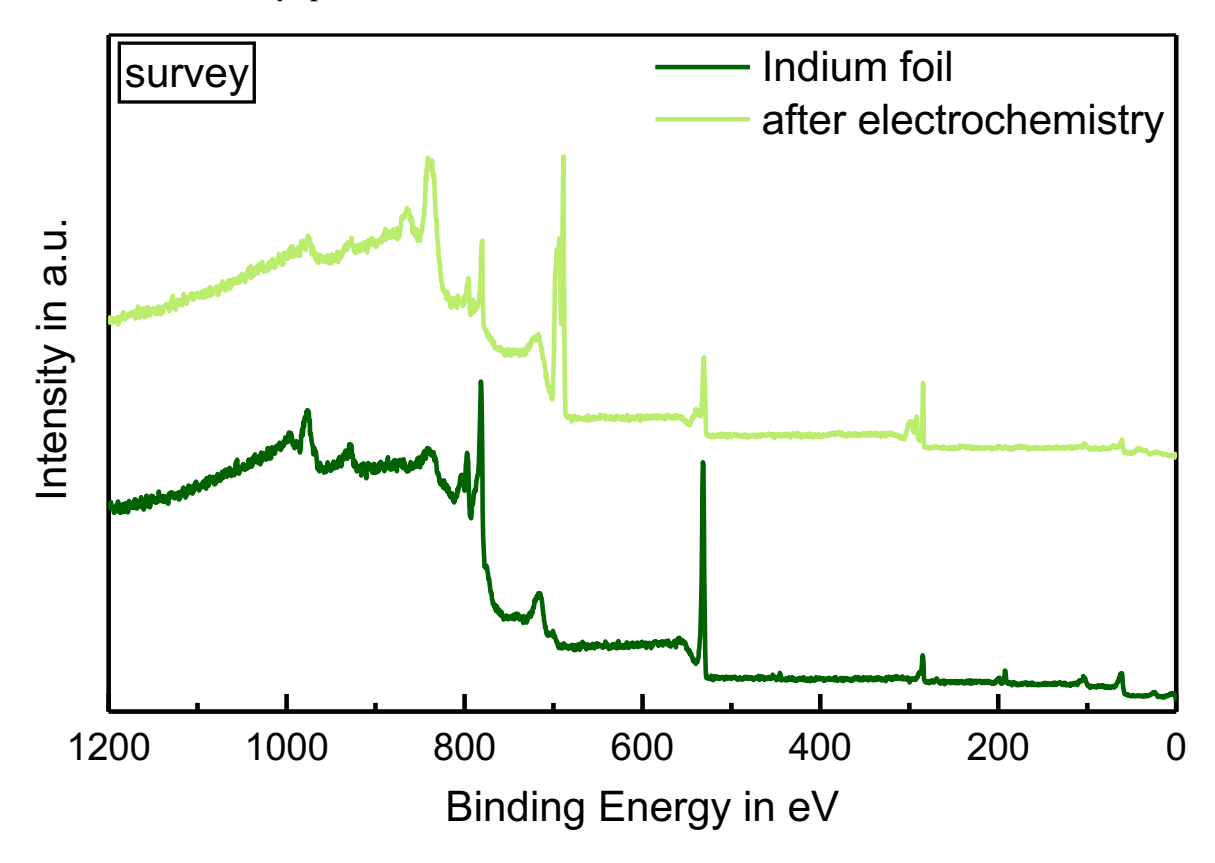


Figure S6: XP survey spectra the Co₃B catalyst before (indium foil) and after electrochemical investigation.

7. Comparison of the catalytic activity of different metal borides for the OER

Table S1: Comparison of the OER catalytic activity of different transition metal borides on flat surfaces in alkaline media from literature.

Material	Electrolyte	Overpotential	Current density	Reference
		in mV	in mA/cm ²	Reference
Co ₃ B / GC	1 M KOH	350	20	This work
Annealed 500-Co ₂ B / GC	1 M KOH	430	20	(4)
Co-B _i	1 M KOH	345	10	(5)
Co-B / Cu	1 M KOH	340	10	(6)
Fe-B / Cu	1 M KOH	472	10	(6)
Annealed 500-Co ₂ B	0.1 M KOH	380	10	(7)
Co-B / GC	1 M KOH	360	10	(8)
Ni-B / GC	1 M KOH	402	10	(8)
Co-B / GC	1 M KOH	322	10	(9)
Ni-B / GC	1 M KOH	314	10	(9)
Fe-B / GC	1 M KOH	365	10	(9)

References

- (1) Fruchart, D.; Chaudouet, P.; Fruchart, R.; Rouault, A.; Senateur, J. P. Etudes structurales de composés de type cémentite: Effet de l'hydrogène sur Fe₃C suivi par diffraction neutronique. Spectrométrie Mössbauer sur FeCo₂B et Co₃B dopés au ⁵⁷Fe. *J. Solid State Chem.* **1984**, *51*, 246-252.
- (2) Owen, E. A.; Madoc Jones, D. Effect of Grain Size on the Crystal Structure of Cobalt. *Proc. Phys. Soc. B* **1954**, *67*, 456-466.
- (3) Doyle, R. L.; Godwin, I. J.; Brandon, M. P.; Lyons, M. E. G. Redox and electrochemical water splitting catalytic properties of hydrated metal oxide modified electrodes. *Phys. Chem. Chem. Phys.* **2013**, *15*, 13737-13783.
- (4) Klemenz, S.; Schuch, J.; Hawel, S.; Zieschang, A.-M.; Kaiser, B.; Jaegermann, W.; Albert, B. Synthesis of a Highly Efficient Oxygen-Evolution Electrocatalyst by Incorporation of Iron into Nanoscale Cobalt Borides. *ChemSusChem* **2018**, *11*, 3150-3156.
- (5) Chen, P.; Xu, K.; Zhou, T.; Tong, Y.; Wu, J.; Cheng, H.; Lu, X.; Ding, H.; Wu, C.; Xie, Y. Strong-Coupled Cobalt Borate Nanosheets/Graphene Hybrid as Electrocatalyst for Water Oxidation Under Both Alkaline and Neutral Conditions. *Angew. Chem. Int. Ed.* **2016**, *55*, 2488-2492.
- (6) Chen, H.; Ouyang, S.; Zhao, M.; Li, Y.; Ye, J. Synergistic Activity of Co and Fe in Amorphous Cox-Fe-B Catalyst for Efficient Oxygen Evolution Reaction. *ACS Appl. Mater. Interfaces* **2017**, *9*, 40333-40343.
- (7) Masa, J.; Weide, P.; Peeters, D.; Sinev, I.; Xia, W.; Sun, Z.; Somsen, C.; Muhler, M.; Schuhmann, W. Amorphous Cobalt Boride (Co₂B) as Highly Efficient Nonprecious Catalyst for Electrochemical Water Splitting: Oxygen and Hydrogen Evolution. *Adv. Energy Mater.* **2016**, *6*, 1502313.
- (8) Zhang, J.; Li, X.; Liu, Y.; Zeng, Z.; Cheng, X.; Wang, Y.; Tu, W.; Pan, M. Bi-metallic boride electrocatalysts with enhanced activity for the oxygen evolution reaction. *Nanoscale* **2018**, *10*, 11997-12002.
- (9) Nsanzimana, J. M. V.; Peng, Y.; Xu, Y. Y.; Thia, L.; Wang, C.; Xia, B. Y.; Wang, X. An Efficient and Earth-Abundant Oxygen-Evolving Electrocatalyst Based on Amorphous Metal Borides. *Adv. Energy Mater.* **2018**, *8*, 1701475.